INTERNATIONAL JOURNAL FOR NUMERICAL METHODS IN ENGINEERING
Int. J. Numer. Meth. Engng. **45**, 693–719 (1999)

COMPUTATIONAL SCHEMES FOR NON-LINEAR ELASTO-DYNAMICS

O. A. BAUCHAU*,† AND T. JOO‡

School of Aerospace Engineering, Georgia Institute of Technology, Atlanta, GA 30332, U.S.A.

SUMMARY

This paper deals with the development of computational schemes for the dynamic analysis of non-linear elastic systems. The focus of the investigation is on the derivation of unconditionally stable time-integration schemes presenting high-frequency numerical dissipation for these types of problem. At first, schemes based on Galerkin and time-discontinuous Galerkin approximations applied to the equations of motion written in the symmetric hyperbolic form are proposed. Though useful, these schemes require casting the equations of motion in the symmetric hyperbolic form, which is not always possible. Furthermore, this approaches to unacceptably high computational costs. Next, unconditionally stable schemes are proposed that do not rely on the symmetric hyperbolic form. Both energy-preserving and energy-decaying schemes are derived. Numerical examples are presented to demonstrate the accuracy and efficiency of the proposed schemes. Copyright © 1999 John Wiley & Sons, Ltd.

KEY WORDS: elastodynamics; integration schemes; energy conservation

1. INTRODUCTION

This paper is concerned with the dynamic analysis of non-linear elastic systems, and more specifically with time-integration schemes for the equations of motion describing their response. The main focus is on the derivation of an algorithm presenting high-frequency numerical dissipation, and for which unconditional stability can be proven in the non-linear case. An energy-decay argument will be used to establish stability [1].

The Newmark family of algorithms [2] is widely used in structural dynamics. In particular, the average acceleration method, also known as the trapezoidal rule, is a second-order-accurate scheme that presents unconditional stability when applied to linear problems. The classical stability analysis of this scheme can be readily found in text books [3] and shows that the spectral radius remains exactly equal to unity at all frequencies. An alternate way of proving stability is based on an energy argument. Indeed, it is easily shown that the average acceleration scheme exactly preserves the total energy of the system [1].

* Correspondence to: O. A. Bauchau, School of Aerospace Engineering, Georgia Institute of Technology, Atlanta, GA 30332-0150, U.S.A. E-mail: olivier.bauchau@ae.gatech.edu
† Professor
‡ Graduate Assistant

CCC 0029–5981/99/180693–27$17.50

Received 14 July 1997
Revised 9 June 1998

For large finite element discretizations, very high frequencies are present in the model and high-frequency numerical dissipation is desirable, if not indispensable. Numerical dissipation cannot be introduced in the Newmark method without degrading the accuracy. Hilber *et al.* [4] introduced the α-method to remedy this situation. More recently, the generalized-α method [5] was introduced that achieves high-frequency dissipation while minimizing unwanted low-frequency dissipation. Both methods have been successfully used for both linear and non-linear problems, though unconditional stability can be proved only for linear systems.

Simo and his co-workers have introduced an energy-preserving algorithm for non-linear elastodynamics [6]. The unconditional stability of these schemes stems from a proof of conservation of the total energy of the system. An energy-preserving scheme for non-linear elastic multi-body systems was proposed by Bauchau [7]. In this scheme, the equations of motion are discretized so that they imply conservation of the total energy for the elastic components of the system, whereas the forces of constraint associated with the kinematic constraints are discretized so that the work they perform vanishes exactly. The combination of these two features of the discretization guarantees the stability of the numerical integration process for non-linear elastic multi-body systems.

Though energy-preserving schemes perform well, their lack of high-frequency numerical dissipation can be a problem [7]. First, the time histories of internal forces and velocities can present a very significant high-frequency content. Second, it seems that the presence of high-frequency oscillations can hinder the convergence process for the solution of the non-linear equations of motion. This was observed in several examples where the dynamic response of the system does involve significant high-frequency content. The selection of a smaller time step does not necessarily help this convergence process, as a smaller time step allows even higher frequency oscillations to be present in the response. Finally, it seems that the presence of high-frequency oscillations also renders strict energy preservation difficult to obtain. This could prove to be a real limitation of energy-preserving schemes when applied to more and more complex models. For such models, the use of integration schemes presenting high-frequency numerical dissipation become increasingly desirable.

It appears that the development of 'energy-decaying' schemes, i.e. schemes eliminating the energy associated with vibratory motions at high frequency, is desirable and often indispensable. This is particularly important when dealing with large-scale elastodynamics problems, or with problems presenting a complex dynamic response.

The key to the development of an energy-decaying scheme is the derivation of an *energy decay inequality* [1] rather that the *discrete energy-conservation law* which is central to energy-preserving schemes. A methodology that can systematically lead to an energy decay inequality is the *time discontinuous Galerkin method* [8–10] which was initially developed for hyperbolic equations. Hughes and Hulbert [11, 12] have investigated the use of the time discontinuous Galerkin methodology for linear elastodynamics. They point out that: 'classical elastodynamics can be converted to first-order symmetric hyperbolic form, which has proved useful in theoretical studies. Finite element methods for first-order symmetric hyperbolic system are thus immediately applicable. However, there seems to be several disadvantages: in symmetric hyperbolic form the state vector consists of displacements, velocities, and stresses which is computationally uneconomical; and the generalization to non-linear elastodynamics seems possible only in special circumstances'. Indeed, writing the non-linear equations of motion of numerous structural elements in this symmetric hyperbolic form does not appear to be possible.

In this paper, an alternate route is taken. Practical time-integration schemes that do not rely on the symmetric hyperbolic form of the equations of motion are developed. These schemes are

finite-difference schemes in nature, and imply an energy balance condition that is obtained by a direct computation of the work done by the discretized inertial and elastic forces over a time step. This energy balance condition is then used to derive energy conservation or energy decay statements providing a rigorous proof of unconditional stability for the scheme.

This paper is organized in the following manner. In Section 2, the symmetric hyperbolic form of the equations of motions will be discussed, and the properties of Galerkin approximations of these equations written in the symmetric hyperbolic form will be presented. Practical time-integration schemes that bypass the need for recasting the equations of motion in the symmetric hyperbolic form will then be introduced in Section 3. Application of the methodology to elastodynamics problems is the subject of Section 4, and finally, numerical examples are presented in the last section.

2. THE SYMMETRIC HYPERBOLIC FORM

2.1. Classical forms of the equations of motion

Consider a dynamical system described by a kinetic energy $\mathscr{K} = \mathscr{K}(\dot{u}_p, u_p)$, and a strain energy $\mathscr{V} = \mathscr{V}(u_p)$, where u_p are the degrees of freedom of the system, and $\dot{(.)}$ denotes a derivative with respect to time. The Lagrangian of the system is defined as $\mathscr{L}(\dot{u}_p, u_p) = \mathscr{K} - \mathscr{V}$, and the equations of motion of the system in Lagrangian form are then

$$\frac{\mathrm{d}}{\mathrm{d}t}(\mathscr{L}_{,\dot{u}_p}) - \mathscr{L}_{,u_p} = 0 \tag{1}$$

The notation $(.)_{,u}$ is used here to indicate a derivative with respect to u, and a summation is implied by repeated indices. Hamilton's formulation is obtained with the help of a Legendre transformation [13]. First, the momenta are defined as $p_p(\dot{u}_r, u_r) = \mathscr{L}_{,\dot{u}_p}$, and these relationships can be inverted to yield $\dot{u}_p = \dot{u}_p(u_r, p_r)$. The Hamiltonian of the system is now defined

$$\mathscr{H}(u_r, p_r) = p_p\ \dot{u}_p(u_r, p_r) - \mathscr{L}(u_r, p_r) \tag{2}$$

The equations of motion of the system in Hamiltonian form are then

$$\dot{u}_p = \mathscr{H}_{,p_p}, \quad \dot{p}_p + \mathscr{H}_{,u_p} = 0 \tag{3}$$

2.2. The symmetric hyperbolic form

The symmetric hyperbolic form stems from a second Legendre transformation. The following variables are first defined:

$$f_p(u_r, p_r) = \mathscr{H}_{,u_p}, \quad v_p(u_r, p_r) = \mathscr{H}_{,p_p} \tag{4}$$

These relations can be inverted to yield $u_p = u_p(f_r, v_r)$ and $p_p = p_p(f_r, v_r)$. A new function is now defined

$$\mathscr{G}(f_r, v_r) = f_p u_p(f_r, v_r) + v_p p_p(f_r, v_r) - \mathscr{H}(f_r, v_r) \tag{5}$$

implying $u_p = \mathscr{G}_{,f_p}$ and $p_p = \mathscr{G}_{,v_p}$. It can be readily shown that the Hessians of $\mathscr{H}$ and $\mathscr{G}$ are the inverse of each other. Hence, if $\mathscr{H}$ is a positive-definite function, so is $\mathscr{G}$. Hamilton's equations

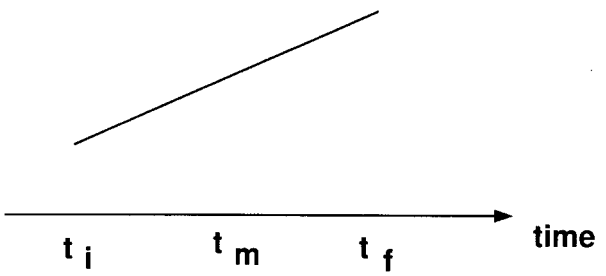

Figure 1. The Galerkin approximation

(3) can be expressed in terms of the new variables f_p and v_p to find the symmetric hyperbolic form of the equations of motion

$$\mathscr{G}_{,f_p f_q}\dot{f}_q + \mathscr{G}_{,f_p v_q}\dot{v}_q - v_p = 0, \quad \mathscr{G}_{,v_p f_q}\dot{f}_q + \mathscr{G}_{,v_p v_q}\dot{v}_q + f_p = 0 \tag{6}$$

To simplify the notation, an implicit form of the equations is preferred:

$$\dot{u}_p(f_r, v_r) - v_p = 0, \quad \dot{p}_p(f_r, v_r) + f_p = 0 \tag{7}$$

2.3. The Galerkin approximation

In the Galerkin approximation, the equations of motion are enforced in a weak, integral manner. Figure 1 shows a time interval from t_i to t_f, and an approximate solution over that interval. Superscripts $(.)^i$ and $(.)^f$ will be used to indicate the value of a quantity at times t_i and t_f, respectively. The Galerkin approximation of the equations of motion in implicit symmetric hyperbolic form (7) is

$$\int_{t_i}^{t_f} \{w_{1p}[\dot{u}_p(f_r, v_r) - v_p] + w_{2p}[\dot{p}_p(f_r, v_r) + f_p]\}\,\mathrm{d}t = 0 \tag{8}$$

where w_{1p} and w_{2p} are arbitrary test functions. Integration by parts yields

$$\int_{t_i}^{t_f} [-\dot{w}_{1p}u_p - \dot{w}_{2p}p_p - w_{1p}v_p + w_{2p}f_p]\,\mathrm{d}t + w_{1p}^f u_p^f + w_{2p}^f p_p^f - w_{1p}^i u_p^i - w_{2p}^i p_p^i = 0 \tag{9}$$

This approximation of the equations of motion enjoys remarkable properties. Indeed, selecting the test functions as $w_{1p} = f_p$ and $w_{2p} = v_p$ yields

$$\int_{t_i}^{t_f} [-\dot{f}_p\mathscr{G}_{,f_p} - \dot{v}_p\mathscr{G}_{,v_p} - f_p v_p + v_p f_p]\,\mathrm{d}t + f_p^f u_p^f + v_p^f p_p^f - f_p^i u_p^i - v_p^i p_p^i = 0 \tag{10}$$

The time integral clearly has a closed-form solution, leading to

$$\mathscr{G}^i - \mathscr{G}^f + f_p^f u_p^f + v_p^f p_p^f - f_p^i u_p^i - v_p^i p_p^i = 0 \tag{11}$$

Finally, we express $\mathscr{G}$ in terms of the Hamiltonian $\mathscr{H}$ with the help of (5) to find

$$\mathscr{H}^f = \mathscr{H}^i \tag{12}$$

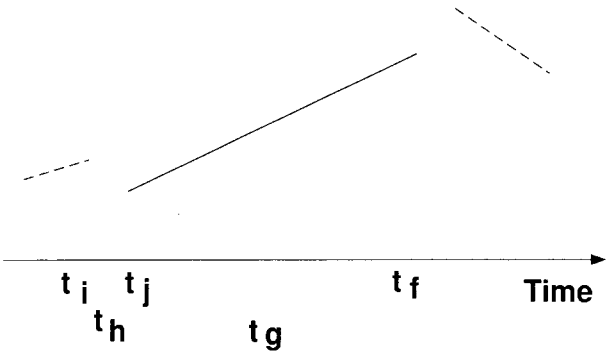

Figure 2. The time discontinuous Galerkin approximation

In summary, the Galerkin approximation (8) of the equations of motion written in symmetric hyperbolic form implies a discrete Hamiltonian conservation statement (12). If the Hamiltonian is a positive-definite function, this statement implies the *unconditional stability* of integration schemes based on (8).

2.4. The time-discontinuous Galerkin approximation

In the time-discontinuous Galerkin approximation, the solution is allowed to present discontinuities in the displacement and velocity fields at discrete times. Figure 2 shows a time interval from t_i to t_f and the approximate solution over that interval. At the initial instant, the solution presents a jump. Superscripts $(.)^i$ will be used to denote the value of a discontinuous quantity on the left side of the jump, whereas a superscript $(.)^j$ indicates the value of that quantity on the right side of the jump. The equations of motion and initial conditions are enforced in a weak, integral manner. The time-discontinuous Galerkin approximation of the equations of motion in implicit symmetric hyperbolic form (7) is

$$\int_{t_j}^{t_f} \{w_{1p}[\dot{u}_p(f_r, v_r) - v_p] + w_{2p}[\dot{p}_p(f_r, v_r) + f_p]\}\,\mathrm{d}t + w_{1p}^j\langle u_p\rangle + w_{2p}^j\langle p_p\rangle = 0 \tag{13}$$

where the notation $\langle . \rangle$ is used to denote the jump in a quantity at the initial time, i.e. $\langle u_p\rangle = u_p^j - u_p^i$ and $\langle p_p\rangle = p_p^j - p_p^i$. This approximation of the equations of motion also enjoys remarkable properties. Indeed, integrating by parts and selecting the test functions as $w_{1p} = f_p$ and $w_{2p} = v_p$ yields

$$\int_{t_j}^{t_f} [-\dot{f}_p \mathscr{G}_{,f_p} - \dot{v}_p \mathscr{G}_{,v_p} - f_p v_p + v_p f_p]\,\mathrm{d}t + f_p^f u_p^f + v_p^f p_p^f - f_p^j u_p^i - v_p^j p_p^i = 0 \tag{14}$$

The time integral clearly has a closed-form solution leading to

$$\mathscr{G}^j - \mathscr{G}^f + f_p^f u_p^f + v_p^f p_p^f - f_p^j u_p^i - v_p^j p_p^i = 0 \tag{15}$$

Finally, we express $\mathscr{G}$ in terms of the Hamiltonian $\mathscr{H}$ with the help of (5) to find

$$\mathscr{H}^f - \mathscr{H}^j + f_p^j\langle u_p\rangle + v_p^j\langle p_p\rangle = 0 \tag{16}$$

Since the Hamiltonian is a continuous function of u_r and p_r, the mean value theorem implies

$$\mathscr{H}^j = \mathscr{H}^i + f_p^j\langle u_p\rangle + v_p^j\langle p_p\rangle - \frac{1}{2}[\mathscr{H}^h_{,u_p u_q}\langle u_p\rangle\langle u_q\rangle + \mathscr{H}^h_{,u_p p_q}\langle u_p\rangle\langle p_q\rangle + \mathscr{H}^h_{,p_p u_q}\langle p_p\rangle\langle u_q\rangle + \mathscr{H}^h_{,p_p p_q}\langle p_p\rangle\langle p_q\rangle] = \mathscr{H}^i + f_p^j\langle u_p\rangle + v_p^j\langle p_p\rangle - c^2 \tag{17}$$

where the last equality holds if the Hamiltonian is a positive-definite function. Combining (16) and (17) then yields

$$\mathscr{H}^f = \mathscr{H}^i - c^2 \Rightarrow \mathscr{H}^f \leqslant \mathscr{H}^i \tag{18}$$

In summary, the time-discontinuous Galerkin approximation (13) of the equations of motion written in symmetric hyperbolic form implies a Hamiltonian decay inequality (18), if the Hamiltonian is a positive-definite quantity. This inequality implies the *unconditional stability* of time-integration schemes based on (13).

2.5. Discussion

Both Galerkin (8) and time-discontinuous Galerkin (13) approximations applied to the equations of motion written in the symmetric hyperbolic form (7) have been shown to provide a systematic way of deriving unconditionally stable time-integration schemes, provided the Hamiltonian is a positive-definite function. It should be noted that this conclusion holds if the spaces of admissible weighting functions w_{1p} and w_{2p} are chosen to coincide with the spaces of admissible functions f_p and v_p, respectively, and equations (8) and (13) are integrated exactly given the choice of admissible functions.

The energy decay inequality associated with the time-discontinuous Galerkin approximation implies the presence of numerical dissipation in the resulting time-integration schemes, whereas such dissipation is ruled out by the strict energy conservation associated with the Galerkin approximation. Since the presence of numerical dissipation is highly desirable, the time-discontinuous Galerkin approach appears to be the most promising method.

However, both of these approaches present major drawbacks. First, it is not always possible to recast the equations of motion of general systems into the symmetric hyperbolic form. For instance, constrained mechanical system, an important class of structural dynamics problems, can clearly not be recast in the symmetric hyperbolic form due to the presence of algebraic equations. Second, even when a symmetric hyperbolic form exists, it will be difficult to exactly evaluate the integrals appearing in equations (8) and (13). Numerical integration, typically used in finite element applications, would not be an option as this approximation would no longer guarantee the unconditional stability of the resulting scheme. Finally, even if these two obstacles were overcome, the time-discontinuous Galerkin approach will result in high computational cost because it requires two level of unknowns (at t_j and t_f). In elastodynamics, three fields are required for the symmetric hyperbolic form: displacements, stresses and momenta. Hence, the final discrete equations will involve $6N$ unknowns, resulting in unacceptably high computational cost [11].

3. PRACTICAL TIME-INTEGRATION SCHEMES

In this section, time-integration schemes applicable to non-linear elastodynamics will be developed, without resorting to the symmetric hyperbolic form of the equations of motion. The investigation

will focus on dynamical system defined by a kinetic energy $\mathscr{K} = 1/2 M_{pq} v_p v_q$ and a strain energy $\mathscr{V} = 1/2 C_{pq} \varepsilon_p \varepsilon_q$. The mass matrix M_{pq} and stiffness matrix C_{pq} are symmetric and positive-definite; the velocities and strains are given as $v_p = R_{pq}(u_r)\dot{u}_q$, and $\varepsilon_p = \varepsilon_p(u_r)$, respectively. Note that the velocities are assumed to be linear functions of the $\dot{u}_p$, resulting in a kinetic energy that is a quadratic form in $\dot{u}_p$. Under these conditions the total mechanical energy of the system is preserved [13].

The equations of motion of such systems simply write $\mathscr{F}^{\mathrm{i}}_p + \mathscr{F}^{\mathrm{e}}_p = \mathscr{F}^{\mathrm{a}}_p(t)$, where $\mathscr{F}^{\mathrm{a}}_p(t)$ are the time-dependent applied forces. The inertial and elastic forces, denoted $\mathscr{F}^{\mathrm{i}}_p$ and $\mathscr{F}^{\mathrm{e}}_p$, respectively, are

$$\mathscr{F}^{\mathrm{i}}_p = \frac{\mathrm{d}}{\mathrm{d}t}(R_{qp} p_q) - \dot{u}_r D_{qpr} p_q, \quad D_{pqr} = R_{pq,r} \tag{19}$$

$$\mathscr{F}^{\mathrm{e}}_p = B_{qp} f_q, \quad B_{pq} = \varepsilon_{p,q} \tag{20}$$

where $p_q = M_{qr} v_r$ and $f_q = C_{qr}\varepsilon_r$. The notation $(.)_{,p}$ indicates a derivative with respect to u_p.

The energy-conservation statement can be obtained by evaluating the work done by the inertial, elastic, and applied forces. The work done by the inertial forces is computed first $\mathscr{W}^{\mathrm{i}} = \int_{t_i}^{t_f} \dot{u}_p \mathscr{F}^{\mathrm{i}}_p \,\mathrm{d}t = \mathscr{K}^f - \mathscr{K}^i$. Next, the work done by the elastic forces is evaluated $\mathscr{W}^{\mathrm{e}} = \int_{t_i}^{t_f} \dot{u}_p \mathscr{F}^{\mathrm{e}}_p \,\mathrm{d}t = \mathscr{V}^f - \mathscr{V}^i$. Finally, the work done by the applied forces is $\mathscr{W}^{\mathrm{a}} = \int_{t_i}^{t_f} \dot{u}_p Q_q \,\mathrm{d}t$. Hence, the equations of motion imply the following work balance equation

$$\mathscr{K}^{\mathrm{f}} - \mathscr{K}^{\mathrm{i}} + \mathscr{V}^{\mathrm{f}} - \mathscr{V}^{\mathrm{i}} = \mathscr{W}^{\mathrm{a}}; \Rightarrow \mathscr{E}^{\mathrm{f}} - \mathscr{E}^{\mathrm{i}} = \mathscr{W}^{\mathrm{a}} \tag{21}$$

where the total mechanical energy $\mathscr{E} = \mathscr{K} + \mathscr{V}$. In the absence of externally applied forces, $\mathscr{W}^{\mathrm{a}} = 0$, and the total energy is preserved.

Our goal is to obtain *discretized* equations of motion that will imply an exact energy conservation condition (21), or an energy decay inequality. At first, discretizations of the inertial and elastic forces are proposed, then energy-preserving and energy-decaying schemes will be derived.

3.1. Discretization of inertial and elastic forces

Consider a time interval t_i, t_f, and an approximate solution over this interval, as shown in Figure 1. The following discretizations of the inertial (19) and elastic (20) forces are proposed:

$$\mathscr{F}^{\mathrm{i}m}_p = \frac{R^f_{qp} p^f_q - R^i_{qp} p^i_q}{\Delta t} - \frac{u^f_r - u^i_r}{\Delta t} D^m_{qrp} \frac{p^f_q + p^i_q}{2} \tag{22}$$

$$\mathscr{F}^{\mathrm{e}m}_p = B^m_{qp} f^m_q \tag{23}$$

where the quantities D^m_{qrp}, B^m_{qp} and f^m_q are as yet undetermined. The work done by the discretized inertial forces is $\mathscr{W}^i = (u^f_p - u^i_p)\mathscr{F}^{\mathrm{i}m}_p$, and regrouping the term yields

$$\mathscr{W}^{\mathrm{i}} = \frac{u^f_p - u^i_p}{\Delta t} \left\{ \left[R^f_{qp} - \frac{u^f_r - u^i_r}{2} D^m_{qpr} \right] p^f_q - \left[R^i_{qp} + \frac{u^f_r - u^i_r}{2} D^m_{qpr} \right] p^i_q \right\} \tag{24}$$

The following condition is now imposed:

$$v_q^m = \left[R_{qp}^f - \frac{u_r^f - u_r^i}{2} D_{qpr}^m \right] \frac{u_p^f - u_p^i}{\Delta t} = \left[R_{qp}^i + \frac{u_r^f - u_r^i}{2} D_{qpr}^m \right] \frac{u_p^f - u^i{}_p}{\Delta t} \tag{25}$$

These relationships now define both D_{qrp}^m and v_p^m. Note that the existence of D_{qrp}^m satisfying (25) is guaranteed by the mean value theorem which states that

$$R_{qp}^f = R_{qp}^i + R_{qp,r}^m (u_r^f - u_r^i) \Rightarrow D_{qpr}^m = R_{qp,r}^m \tag{26}$$

The work done by the discretized inertial forces now becomes $\mathscr{W}^i = (v_q^f - v_q^i) M_{qp} v_p^m$.

Next, the work done by the discretized elastic forces is evaluated: $\mathscr{W}^e = (u_p^f - u_p^i) B_{qp}^m f_q^m$. The following condition is now imposed:

$$\varepsilon_q^f - \varepsilon_q^i = B_{qp}^m (u_p^f - u_p^i) \tag{27}$$

This relationship defines B_{qp}^m. Here again, the existence of B_{qp}^m satisfying this condition is guaranteed by the mean value theorem which states that

$$\varepsilon_q^f = \varepsilon_q^i + \varepsilon_{q,r}^m (u_r^f - u_r^i); \Rightarrow B_{qr} = \varepsilon_{q,r}^m \tag{28}$$

The work done by the discretized elastic forces now becomes $\mathscr{W}^e = (\varepsilon_p^f - \varepsilon_p^i)\ f_p^m$.

3.2. Energy-preserving scheme

The discretized equations of motion for the energy-preserving scheme are

$$\mathscr{F}_p^{im} + \mathscr{F}_p^{em} = \mathscr{F}_p^{am} \tag{29}$$

where $\mathscr{F}_p^{im}$ and $\mathscr{F}_p^{em}$ are now given by (22) and (23), respectively; and $\mathscr{F}_p^{am} = 1/2 \int_{-1}^{+1} \mathscr{F}_p^a(\tau)\, d\tau$. The work done by these discretized forces can be evaluated, as was done in Section 3.1. With the help conditions of (25) and (27) equations of motion (29) imply a work balance statement

$$(v_q^f - v_q^i) M_{pq} v_p^m + (\varepsilon_p^f - \varepsilon_p^i) f_p^m = \mathscr{W}^{am} \tag{30}$$

The following algorithmic velocity–displacement and force–strain relationship are now selected:

$$v_p^m = \frac{v_p^f + v_p^i}{2}, \quad f_p^m = C_{pq} \frac{\varepsilon_p^f + \varepsilon_p^i}{2} \tag{31}$$

The work balance equation (30) then becomes

$$\mathscr{K}^f - \mathscr{K}^i + \mathscr{V}^f - \mathscr{V}^i = \mathscr{W}^a; \Rightarrow \mathscr{E}^f - \mathscr{E}^i = \mathscr{W}^a \tag{32}$$

In summary, discretization (29) implies the energy-conservation statement (32) provided that relationships (25) and (27) are satisfied, and that the algorithmic velocity–displacement and force–strain relationships (31) are used. The scheme can be cast as N non-linear equations for the N degrees of freedom of the problem. The velocities are computed from equation (31).

3.3. Energy-decaying scheme

The discretized equations of motion for the energy-decaying scheme are

$$\mathscr{F}_p^{\mathrm{i}m} + \mathscr{F}_p^{\mathrm{e}g} = \mathscr{F}_p^{\mathrm{a}g}, \qquad \mathscr{F}_p^{\mathrm{i}h} - \tfrac{1}{3}[\mathscr{F}_p^{\mathrm{e}g} - B_{qp}^h f_q^j] = \mathscr{F}_p^{\mathrm{a}h} \tag{33}$$

where $\mathscr{F}_p^{\mathrm{i}m}$, and $\mathscr{F}_p^{\mathrm{i}h}$ are given by (22) using superscripts $(.)^f$, $(.)^i$ and $(.)^j$, $(.)^i$, respectively; $\mathscr{F}_p^{\mathrm{e}g}$ is given by (23) using superscripts $(.)^f$, $(.)^j$; and $\mathscr{F}_p^{\mathrm{a}g} = 1/2 \int_{-1}^{1} \mathscr{F}_p^{\mathrm{a}} \mathrm{d}\tau$ and $\mathscr{F}_p^{\mathrm{a}h} = 1/2 \int_{-1}^{+1} \mathscr{F}_p^{\mathrm{a}} \tau \, \mathrm{d}\tau$.

The work done by the discretized inertial forces is $\mathscr{W}^{\mathrm{i}} = (u_p^f - u_p^i)\mathscr{F}_p^{\mathrm{i}m} + 3\langle u_p \rangle \mathscr{F}_p^{\mathrm{i}h}$. With the help of condition (25) this becomes

$$\mathscr{W}^{\mathrm{i}} = v_p^m M_{pq}(v_q^f - v_q^i) + 3 v_p^h M_{pq} \langle v_q \rangle \tag{34}$$

The work done by the discretized elastic forces is $\mathscr{W}^{\mathrm{e}} = (u_p^f - u_p^i)\mathscr{F}_p^{\mathrm{e}g} - \langle u_p \rangle [\mathscr{F}_p^{\mathrm{e}g} - B_{qp}^h f_q^j]$. With the help of condition (27) this becomes

$$\mathscr{W}^{\mathrm{e}} = (\varepsilon_p^f - \varepsilon_p^j) f_p^g + \langle \varepsilon_p \rangle f_p^j \tag{35}$$

The following velocity–displacement and force–strain relationship are now selected:

$$v_p^m = \frac{v_p^f + v_p^j}{2}, \quad 3v_p^h = -\frac{v_p^f - v_p^j}{2}, \quad f_p^g = C_{pq} \frac{\varepsilon_p^f + \varepsilon_p^j}{2} \tag{36}$$

The work balance equation now is

$$\mathscr{E}^f - \mathscr{E}^j + v_p^j M_{pq} \langle v_q \rangle + f_p^j \langle \varepsilon_p \rangle = \mathscr{W}^{\mathrm{a}} \tag{37}$$

which mirrors (16). Since the total mechanical energy is a positive-definite function of the velocities and strains, the mean value theorem implies

$$\begin{aligned} \mathscr{E}^j = \mathscr{E}^i + v_p^j M_{pq} \langle v_q \rangle + f_p^j \langle \varepsilon_p \rangle - \frac{1}{2}[\mathscr{E}^h_{,v_p v_q} \langle v_p \rangle \langle v_q \rangle + \mathscr{E}^h_{,v_p \varepsilon_q} \langle v_p \rangle \langle \varepsilon_q \rangle \\ + \mathscr{E}^h_{,\varepsilon_p v_q} \langle \varepsilon_p \rangle \langle v_q \rangle + \mathscr{E}^h_{,\varepsilon_p \varepsilon_q} \langle \varepsilon_p \rangle \langle \varepsilon_q \rangle] = \mathscr{E}^i + v_p^j M_{pq} \langle v_q \rangle + f_p^j \langle \varepsilon_p \rangle - c^2 \end{aligned} \tag{38}$$

which is equivalent to (17). Combining (37) and (38) then finally yields

$$\mathscr{E}^f = \mathscr{E}^i - c^2 + \mathscr{W}^{\mathrm{a}}; \;\Rightarrow\; \mathscr{E}^f \leqslant \mathscr{E}^i + \mathscr{W}^{\mathrm{a}} \tag{39}$$

In summary, discretization (33) implies the energy decay statement (39) provided that relationships (25) and (27) are satisfied, and that the algorithmic velocity–displacement and force-strain relationships (36) are used. The scheme can be cast as $2N$ non-linear equations for the N degrees of freedom of the problem at times t_j and t_f. The velocities are computed from equation (36).

3.4. Example: non-linear spring–mass system

Consider the non-linear spring–mass oscillator defined by a kinetic energy $\mathscr{K} = 1/2 m\dot{u}^2$, a strain energy $\mathscr{V} = 1/2 k\varepsilon^2$, and a strain $\varepsilon = u^2$. For this example $m = k = 1{\cdot}0$. It is clear that condition (27) implies $B^m = u^f + u^i$ in this case, and $f^m = k(\varepsilon^f + \varepsilon^i)/2$. The discretized equations of motion

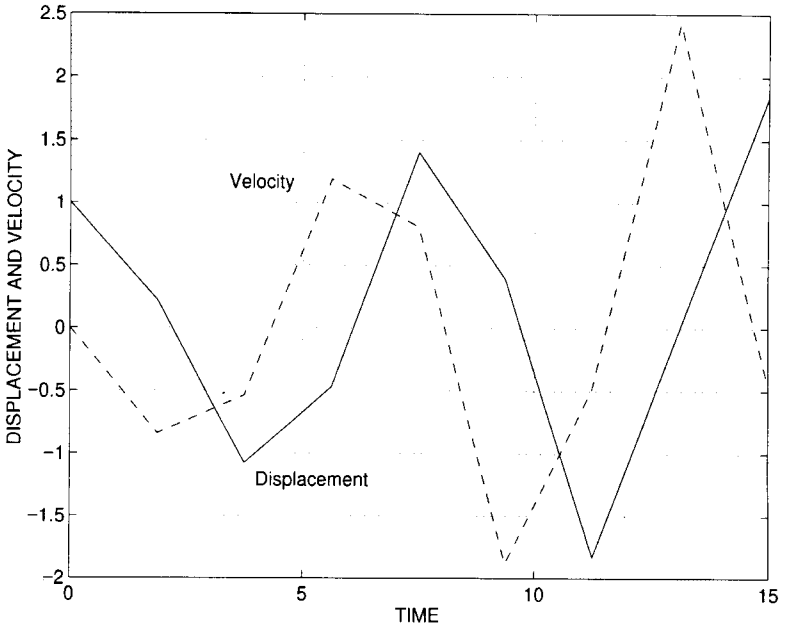

Figure 3. Displacement response for the trapezoidal rule ($u_i = 1{\cdot}0$)

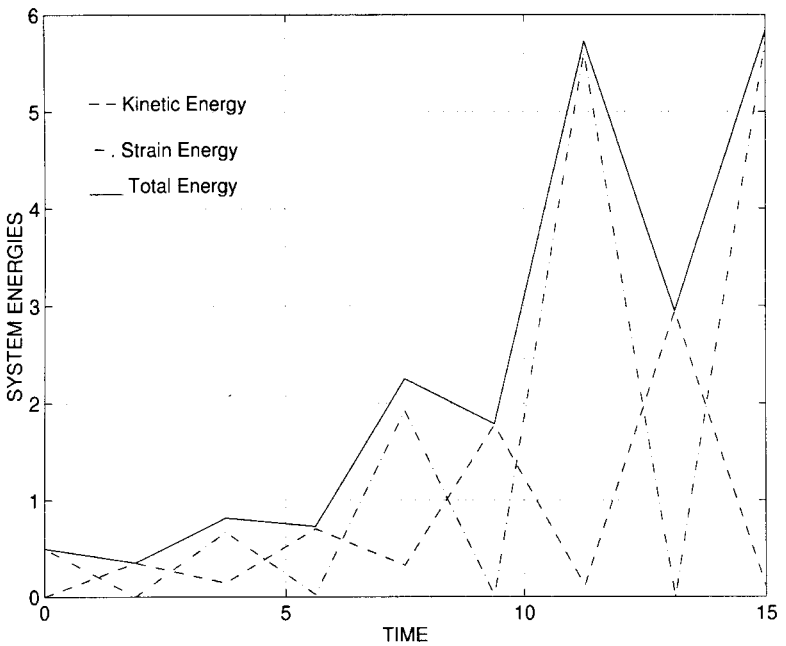

Figure 4. Energy response for the trapezoidal rule ($u_i = 1{\cdot}0$)

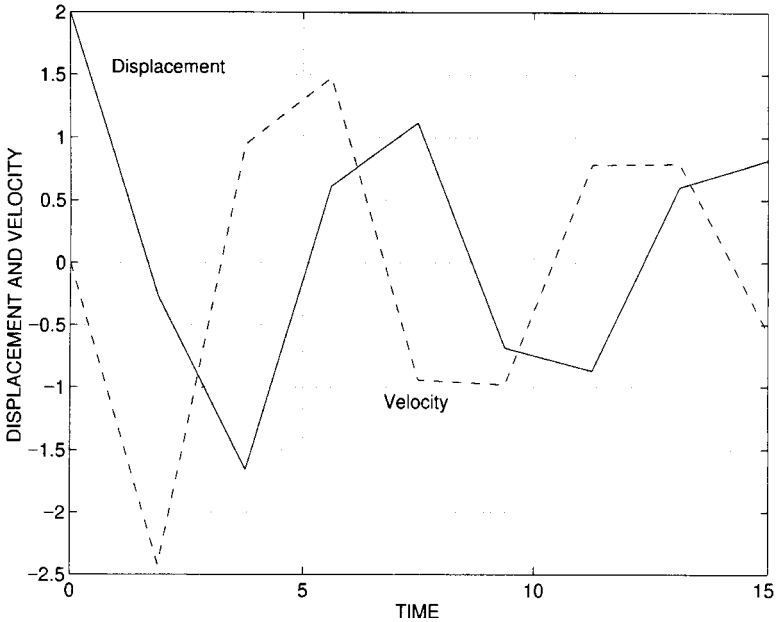

Figure 5. Displacement response for the trapezoidal rule ($u_i = 2{\cdot}0$)

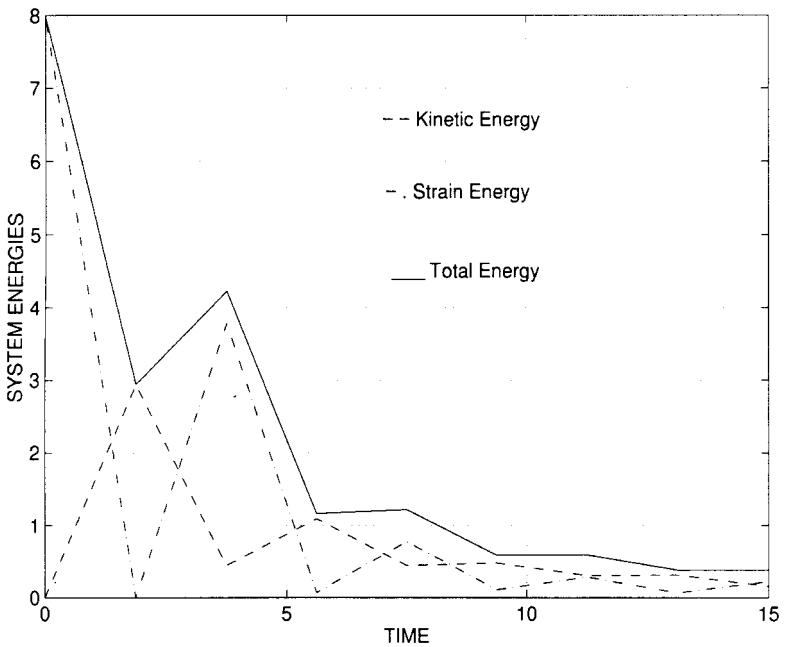

Figure 6. Energy response for the trapezoidal rule ($u_i = 2{\cdot}0$)

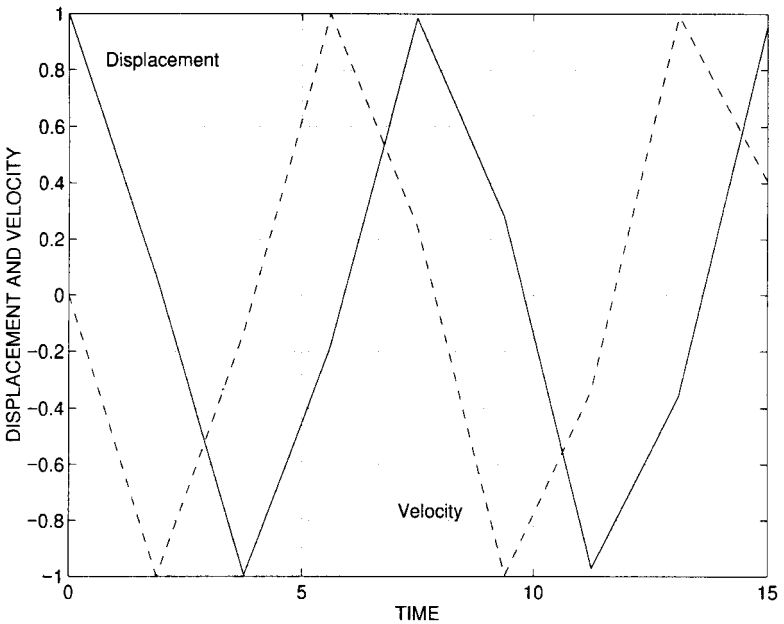

Figure 7. Displacement response for the energy-preserving scheme

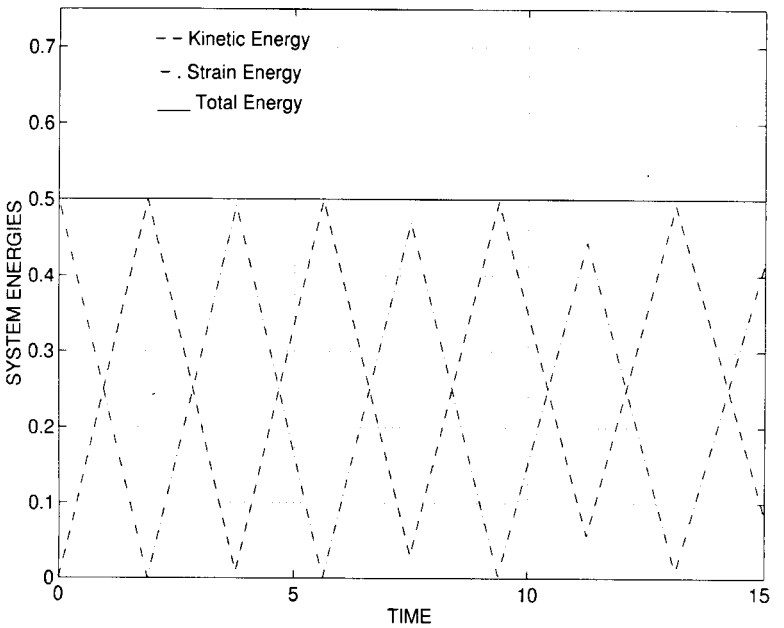

Figure 8. Energy response for the energy-preserving scheme

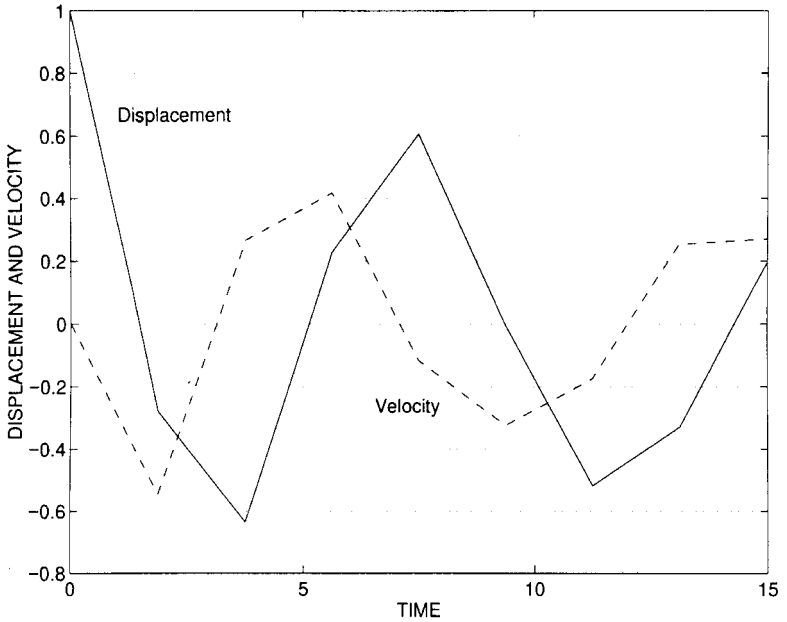

Figure 9. Displacement response for the energy-decaying scheme

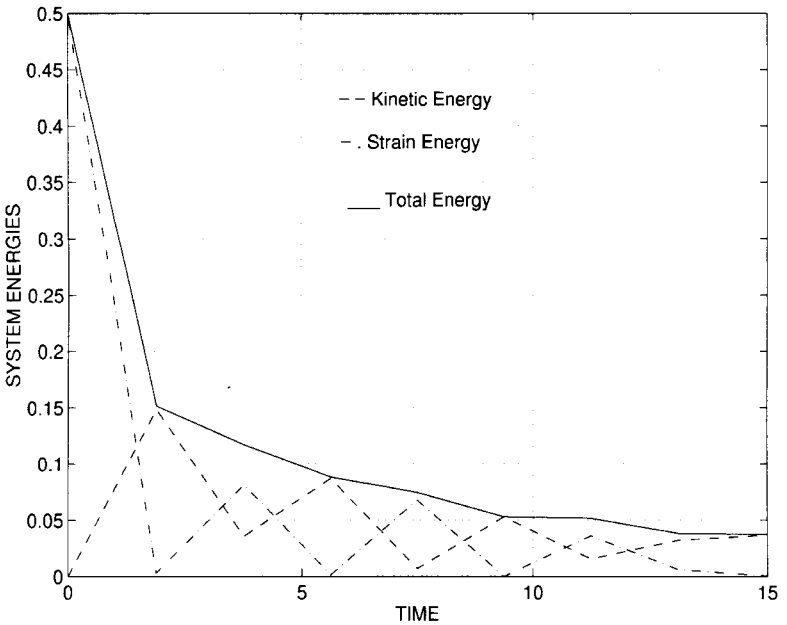

Figure 10. Energy response for the energy-decaying scheme

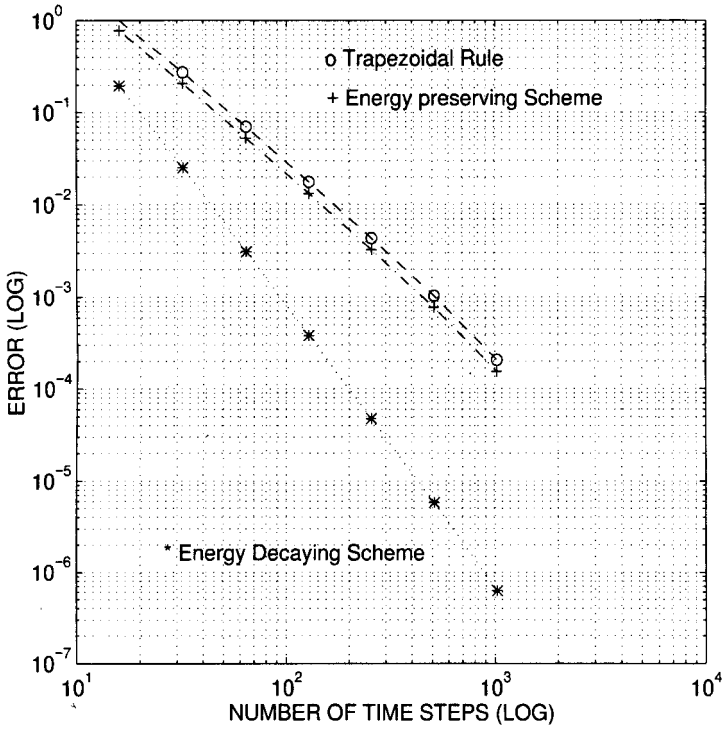

Figure 11. Convergence study

using the trapezoidal rule, the energy-decaying scheme, and the energy-preserving scheme are

$$\frac{mv^f - mv^i}{\Delta t} + 2k\left(\frac{u^f + u^i}{2}\right)^3 = 0 \tag{40}$$

$$\frac{mv^f - mv^i}{\Delta t} + B^m f^m = 0 \tag{41}$$

and

$$\frac{mv^f - mv^i}{\Delta t} + B^g f^g = 0, \quad \frac{mv^j - mv^i}{\Delta t} - \frac{1}{3}[B^g f^g - B^h k \varepsilon^j] = 0 \tag{42}$$

respectively.

Though the trapezoidal rule scheme is unconditionally stable for linear system, there is no guarantee of stability when applied to non-linear systems. Figure 3 shows the response of the system for initial conditions $u_0 = 1{\cdot}0$, $v_0 = 0{\cdot}0$. The total energy rapidly increases as shown by Figure 4. For initial conditions $u_0 = 2{\cdot}0$, $v_0 = 0{\cdot}0$, the corresponding results are shown in Figures 5 and 6, which now show a rapid decrease in energy. The responses predicted by the energy-preserving scheme are shown in Figures 7 and 8; as expected, the total energy of the system is exactly preserved. Finally, Figures 9 and 10 show the responses predicted by the energy-decaying scheme; the total energy of the system decays, as expected. The results of a convergence study shown

in Figure 11 indicate second-order accuracy for the trapezoidal rule and the energy-preserving scheme, and third-order accuracy for the energy-decaying scheme.

4. APPLICATION TO ELASTODYNAMICS

4.1. Equations of motion

The governing equations for elastodynamics is

$$(\rho_0 \dot{u}_p)^{\cdot} - [(\delta_{pq} + u_{p,q})\sigma_{rq}]_{,r} = b_p \tag{43}$$

where ρ_0 is the material density in the reference state, u_p the components of the displacement vector, σ_{pq} the components of the second Piola–Kirchhoff stress tensor, and b_p the components of the externally applied load per unit volume of the reference configuration. Linear constitutive laws will be assumed here between the second Piola–Kirchhoff stress and Green–Lagrange strain tensors

$$\sigma_{pq} = c_{pqrs}\varepsilon_{rs} \tag{44}$$

where ε_{pq} are the components of the Green–Lagrange strain tensor defined as

$$\varepsilon_{pq} = \tfrac{1}{2}(u_{p,q} + u_{q,p} + u_{r,p}u_{r,q}) \tag{45}$$

It can be readily shown that these equations imply an energy-conservation statement $\mathscr{E}^{\mathrm{f}} = \mathscr{E}^{\mathrm{i}} + \mathscr{W}^{\mathrm{a}}$, where the total mechanical energy $\mathscr{E} = \mathscr{K} + \mathscr{V}$. The kinetic and strain energies of the system are

$$\mathscr{K} = \frac{1}{2}\int_v \rho_0 \dot{u}_p \dot{u}_p \,\mathrm{d}v, \quad \mathscr{V} = \frac{1}{2}\int_v c_{pqrs}\varepsilon_{pq}\varepsilon_{rs}\,\mathrm{d}v \tag{46}$$

respectively, where v is the volume of the body in the reference state. Time-integration schemes presenting this energy–conservation property in a discrete sense will now be derived based on the developments of Section 3.

4.2. Discretization of inertial and elastic forces

The following discretization of the inertial forces is proposed:

$$\mathscr{F}_p^{\mathrm{im}} = \rho_0 \frac{v_p^f - v_p^i}{\Delta t} \tag{47}$$

which corresponds to equation (22), specialized to elastodynamics. Indeed, $R_{pq} = \delta_{pq}$ and $D_{pqr} = 0$ for this case. The work done by these inertial forces is now

$$\mathscr{W}^{\mathrm{i}} = \int_v (u_p^f - u_p^i)\rho_0 \frac{v_p^f - v_p^i}{\Delta t}\,\mathrm{d}v \tag{48}$$

As in equation (25), the following definition is now made $v_p^m = (u_p^f - u_p^i)/\Delta t$, and the work done by the inertial forces becomes

$$\mathscr{W}^{\mathrm{i}} = \int_v v_p^m \rho_0 (v_p^f - v_p^i)\,\mathrm{d}v \tag{49}$$

The discretization of the elastic forces mirrors the discretization in equation (23),

$$\mathscr{F}_p^{em} = -[(\delta_{pq} + u_{p,q}^m)\sigma_{rq}^m]_{,r} \tag{50}$$

where $u_p^m = 1/2(u_p^f + u_p^i)$. The work done by these elastic forces is now

$$\mathscr{W}^e = \int_v -(u_p^f - u_p^i)[(\delta_{pq} + u_{p,q}^m)\sigma_{rq}^m]_{,r}\,\mathrm{d}v \tag{51}$$

Integrating by parts and taking advantage of the symmetry of the second Piola–Kirchhoff stress tensor then leads to

$$\mathscr{W}^e = \int_v (\varepsilon_{pq}^f - \varepsilon_{pq}^i)\sigma_{pq}^m\,\mathrm{d}v \tag{52}$$

4.3. Energy-preserving scheme

The discretized equations of motion for the energy-preserving scheme are

$$\rho_0 \frac{v_p^f - v_p^i}{\Delta t} - [(\delta_{pq} + u_{p,q}^m)\sigma_{rq}^m]_{,r} = b_p^m \tag{53}$$

The work done by the discretized forces is readily evaluated with the help of equations (49) and (52) to find

$$\int_v [(v_p^f - v_p^i)\rho_0 v_p^m + (\varepsilon_{pq}^f - \varepsilon_{pq}^i)\sigma_{pq}^m]\,\mathrm{d}v = \mathscr{W}^{am} \tag{54}$$

The following algorithmic velocity–displacement and stress–strain relationships are now selected:

$$v_p^m = \frac{v_p^f + v_p^i}{2}, \quad \sigma_{pq}^m = c_{pqrs}\frac{\varepsilon_{pq}^f + \varepsilon_{pq}^i}{2} \tag{55}$$

which mirrors equation (31). The work balance equation (54) finally becomes

$$(\mathscr{K}^f - \mathscr{K}^i) + (\mathscr{V}^f - \mathscr{V}^i) = \mathscr{W}^a; \quad \Rightarrow \mathscr{E}^f - \mathscr{E}^i = \mathscr{W}^a \tag{56}$$

In summary, discretization (53) of the equations of motion of non-linear, three-dimensional elastodynamics implies the energy conservation statement (56) provided that the algorithmic velocity–displacement and stress–strain relationships (55) are used. This scheme is identical to that proposed by Simo [6].

4.4. Energy-decaying scheme

The discretized equations of motion for the energy-decaying scheme are

$$\rho_0 \frac{v_p^f - v_p^i}{\Delta t} - [(\delta_{pq} + u_{p,q}^g)\sigma_{rq}^g]_{,r} = b_p^g \tag{57}$$

$$\rho_0 \frac{v_p^j - v_p^i}{\Delta t} + \frac{1}{3}[(\delta_{pq} + u_{p,q}^g)\sigma_{rq}^g - (\delta_{pq} + u_{p,q}^h)\sigma_{rq}^j]_{,r} = b_p^g \tag{58}$$

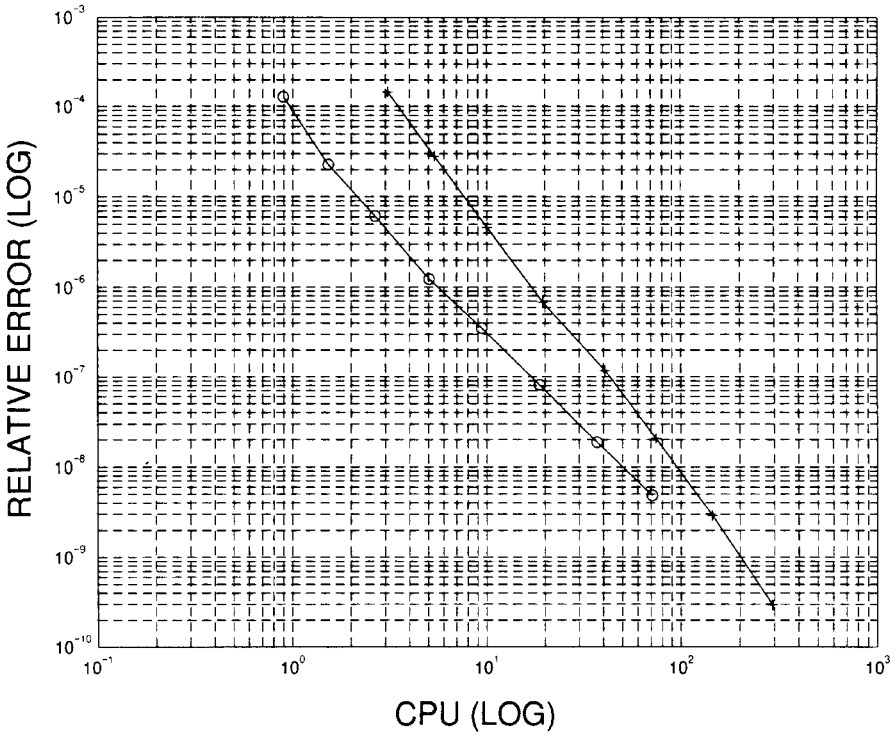

Figure 12. Relative error in tip displacement as a function of CPU time for the energy–preserving (○) and decaying (+) schemes

The total work done by the inertial forces is evaluated using equation (49) to find

$$\mathscr{W}^{\mathrm{i}} = \int_v [v_p^m \rho_0 (v_p^f - v_p^i) + 3 v_p^h \rho_0 \langle v_p \rangle] \, \mathrm{d}v \tag{59}$$

Similarly, the total work done by the elastic forces follows from equation (52):

$$\mathscr{W}^{\mathrm{e}} = \int_v [(\varepsilon_{pq}^f - \varepsilon_{pq}^j)\sigma_{pq}^g + \langle \varepsilon_{pq} \rangle \sigma_{pq}^j] \, \mathrm{d}v \tag{60}$$

The following algorithmic velocity–displacement and stress–strain relationships are now selected:

$$v_p^m = \frac{v_p^f + v_p^j}{2}, \quad 3v_p^h = -\frac{v_p^f - v_p^j}{2}, \quad \sigma_{pq}^g = c_{pqrs} \frac{\varepsilon_{pq}^f + \varepsilon_{pq}^j}{2} \tag{61}$$

as was done in equation (36). The work balance for the system now is

$$\mathscr{E}^f - \mathscr{E}^j + \int_v [v_p^j \rho_0 \langle v_p \rangle + \sigma_{pq}^j \langle \varepsilon_{pq} \rangle] \, \mathrm{d}v = \mathscr{W}^{\mathrm{a}} \tag{62}$$

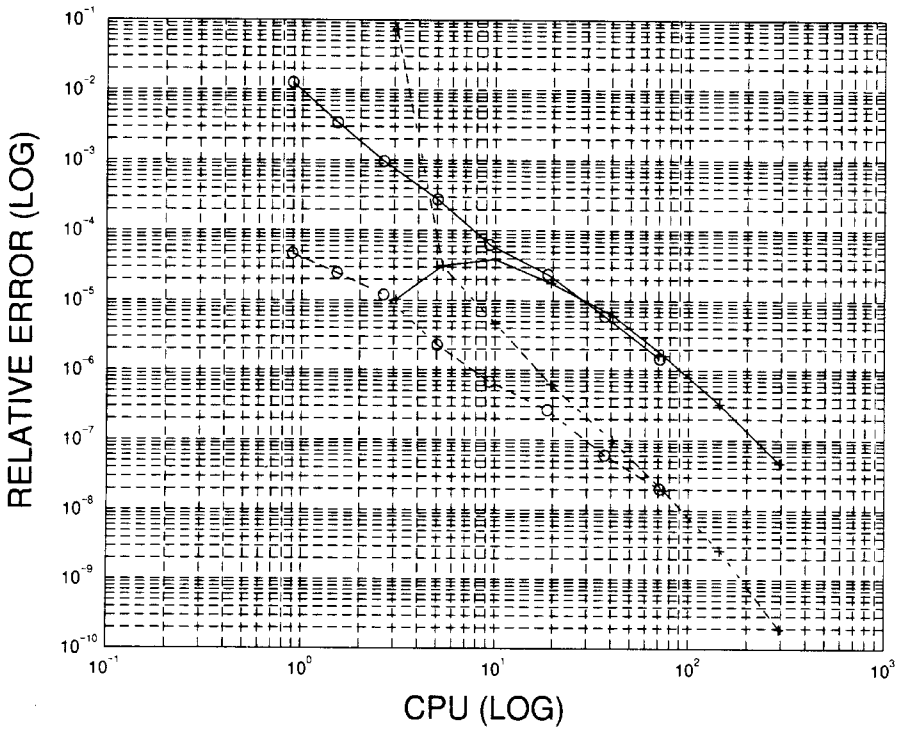

Figure 13. Relative error in tip velocity (dashed line) and root stress (solid line) as a function of CPU time for the energy–preserving (○) and decaying (+) schemes

Since the total mechanical energy is a positive-definite function of the velocities and strains, it is easily shown that

$$\mathscr{E}^j - \mathscr{E}^i - \int_v [v_p^j \rho_0 \langle v_p \rangle + \sigma_{pq}^j \langle \varepsilon_{pq} \rangle] \, \mathrm{d}v = c^2 \tag{63}$$

where the positive quantity c^2 is the numerically dissipated energy

$$c^2 = \frac{1}{2} \int_v [\rho_0 \langle v_p \rangle \langle v_p \rangle + \langle \varepsilon_{pq} \rangle c_{pqrs} \langle \varepsilon_{rs} \rangle] \, \mathrm{d}v \tag{64}$$

This relationship mirrors Eq. (38) which was obtained with the help of the mean value theorem. Combining (62) and (64) then finally yields

$$\mathscr{E}^f = \mathscr{E}^i - c^2 + \mathscr{W}^a; \;\Rightarrow\; \mathscr{E}^f \leqslant \mathscr{E}^i + \mathscr{W}^a \tag{65}$$

In summary, discretizations (57) and (58) of the equations of motion of non-linear, three-dimensional elastodynamics imply the energy decay statement (65) provided that the algorithmic velocity–displacement and stress–strain relationships (61) are used.

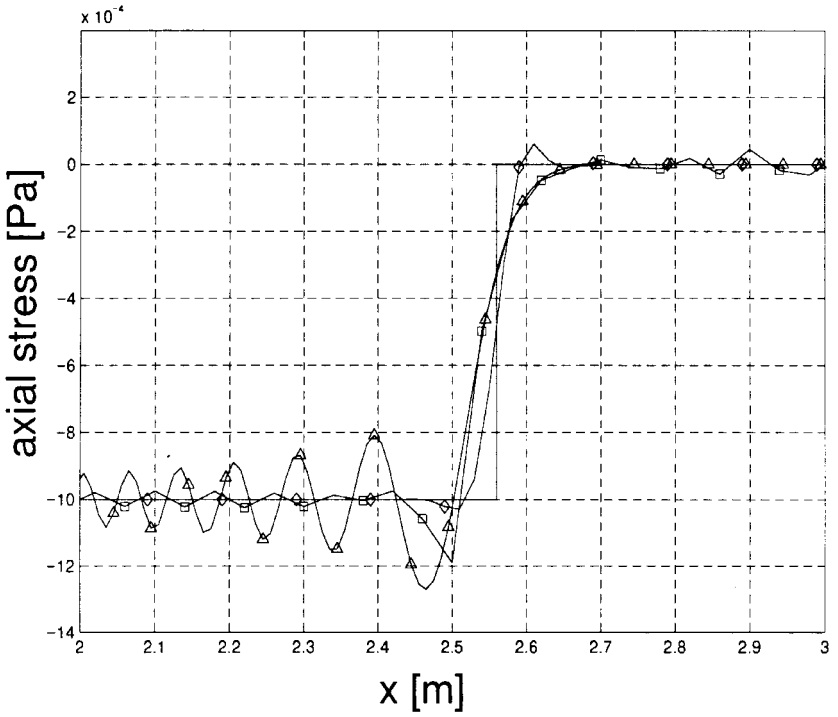

Figure 14. Axial stress distribution in the bar at time $t = 2{\cdot}56\,\mathrm{s}$ using the energy–preserving scheme with three different meshes: 200 (□), 400 (◇), and 800 (△) 9-noded elements

4.5. *General constitutive laws*

Both energy–preserving and decaying schemes were presented in the previous sections for materials that present a linear relationship between the components of the second Piola–Kirchhoff stress tensor and Green–Lagrange strain tensors, i.e. the Saint Venant–Kirchhoff model. For general hyperelastic materials [14], a strain energy density function $a(\varepsilon_{pq})$ is assumed to exist such that

$$\sigma_{pq} = \frac{\partial a}{\partial \varepsilon_{pq}} \tag{66}$$

Within the framework of the energy–preserving scheme, the work done by the elastic forces per unit volume of the reference configuration is $(\varepsilon^f_{pq} - \varepsilon^i_{pq})\sigma^m_{pq}$. Within the time step, the strain is approximated in the following manner:

$$\varepsilon^\eta_{pq} = \frac{\varepsilon^f_{pq} + \varepsilon^i_{pq}}{2} + \frac{\varepsilon^f_{pq} - \varepsilon^i_{pq}}{2}\eta \tag{67}$$

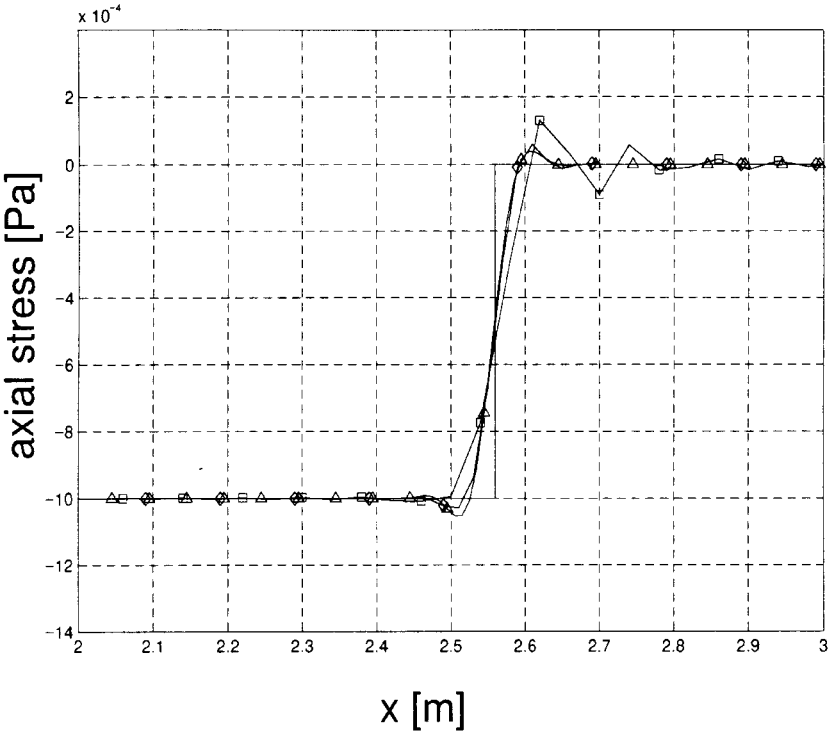

Figure 15. Axial stress distribution in the bar at time $t = 2{\cdot}56$ s using the energy–decaying scheme with three different meshes: 200 (□), 400 (◇), and 800 (△) 9-noded elements

The mean value theorem applied to $a = a(\eta)$ then implies the existence of $-1 \leqslant \hat{\eta} \leqslant 1$ such that

$$a(\varepsilon_{pq}^f) = a(\varepsilon_{pq}^i) + 2 \left. \frac{da(\eta)}{d\eta} \right|_{\hat{\eta}} = a(\varepsilon_{pq}^i) + \sigma_{pq}^m (\varepsilon_{pq}^f - \varepsilon_{pq}^i) \tag{68}$$

where $\sigma_{pq}^m = \sigma_{pq}^{\hat{\eta}}$. It now follows that the work done by the elastic forces is $(\varepsilon_{pq}^f - \varepsilon_{pq}^i)\ \sigma_{pq}^m = a(\varepsilon_{pq}^f) - a(\varepsilon_{pq}^i)$, and Eq. (56) holds again. Hence, in the presence of hyperelastic materials, the algorithmic constitutive law (55) is replaced by (68). This procedure follows that proposed by Simo [6]. Clearly, it can be readily used within the framework of the energy-decaying scheme by replacing the superscripts f and i by f and j, respectively.

5. NUMERICAL EXAMPLES

The following examples illustrate the proposed energy–preserving and decaying formulations. All examples used rectangular, two-dimensional plane strain elements with a consistent mass matrix. Classical iterative procedures were used to solve the non-linear discretized equations.

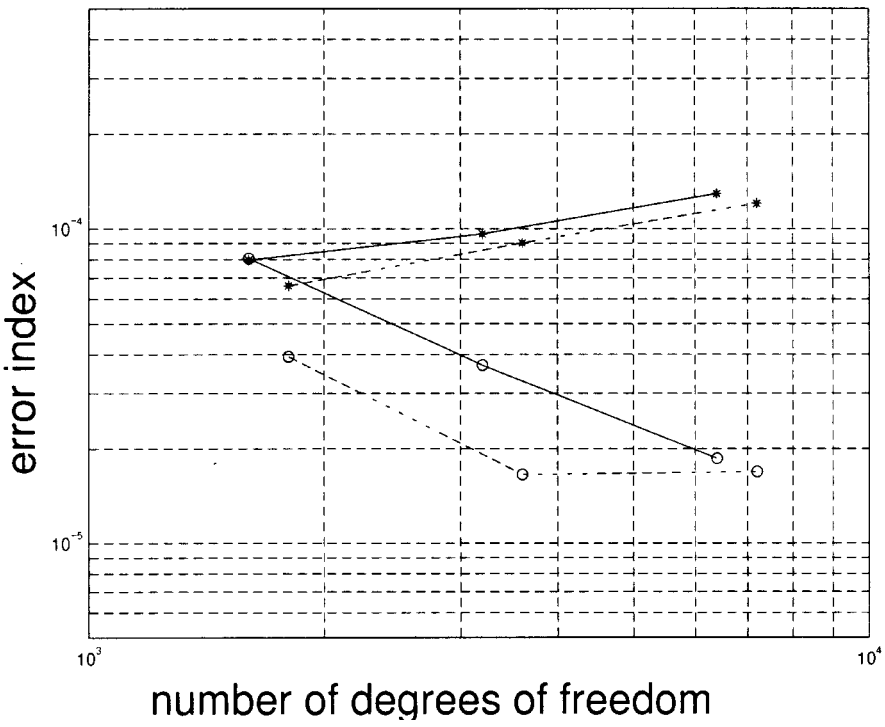

Figure 16. Error index for the various meshes (solid line: 4-noded elements; dashed line: 9-noded elements) using the energy–preserving (∗) and decaying (○) schemes

5.1. The cantilevered beam problem

The first numerical example deals with the dynamic response of a cantilevered beam subjected to a vertical tip load and will be used to demonstrate the convergence characteristics of the proposed schemes. The beam has a length $L = 20\,\text{m}$, a depth $h = 1\,\text{m}$, and a thickness of $t = 1\,\text{m}$. Material properties are: Young's modulus $E = 73\,\text{GPa}$, Poisson's ratio $v = 0{\cdot}3$, and densisty $\rho = 2700\,\text{kg/m}^3$. A tip load $6\,[1-\cos(2\pi t/0{\cdot}8)]\,\text{MN}$ is applied at the tip of the beam. The beam was modelled with eight 8-noded rectangular elements. This problem was studied for a total time of $0{\cdot}4\,\text{s}$ successively divided into 50, 100, 200, 400, 800, 1600, 3200, and 6400 equal time steps. Since no exact solution is available for this problem, the solution obtained with the smallest time step was used as a reference solution and relative errors with respect to this reference were computed for the various simulations.

Figure 12 shows the relative error in tip displacement as a function of the CPU time on a log-log scale. Figure 13 shows the corresponding results for the relative error in beam tip velocity and root stress vector norms. This figure shows that for a given CPU time, similar accuracies are obtained for both velocities and stresses using either energy–preserving or decaying schemes. For a given time step, the energy–decaying scheme is more expensive than the energy–preserving scheme as it involves the solution of $2N$ unknowns instead of N. This handicap is compensated for by the cubic convergence characteristic of the energy-decaying scheme, as compared with the quadratic convergence of the energy-preserving scheme.

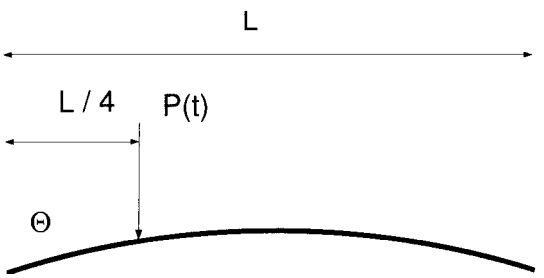

Figure 17. The arch problem

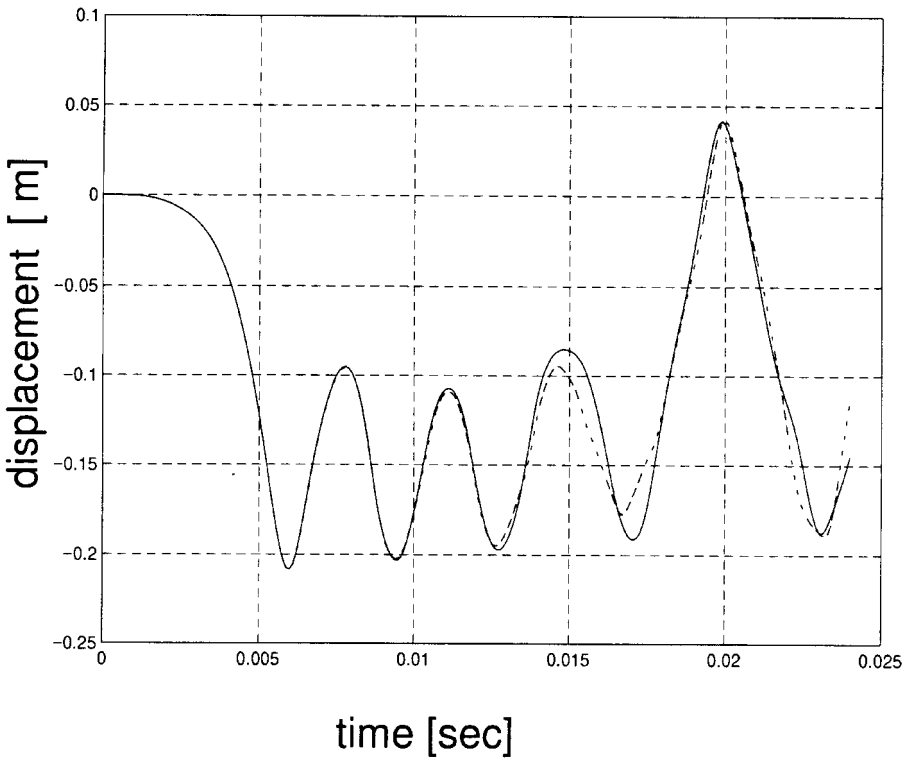

Figure 18. Time history of the mid-span vertical displacement of the arch for the energy–preserving (dashed line) and decaying (solid line) schemes

5.2. Bar impact problem

The second numerical example deals with a homogeneous, two-dimensional bar travelling at a constant velocity $v_0 = 10^{-03}$ m/s to the left and impacting a rigid wall at time $t = 0$. This impact generates a compressive wave in the bar which travels at a constant velocity from the left to the right end of the bar. The bar has a length of 4 m, a Young's modulus $E = 1{\cdot}0\,\mathrm{N/m^2}$, Poisson's

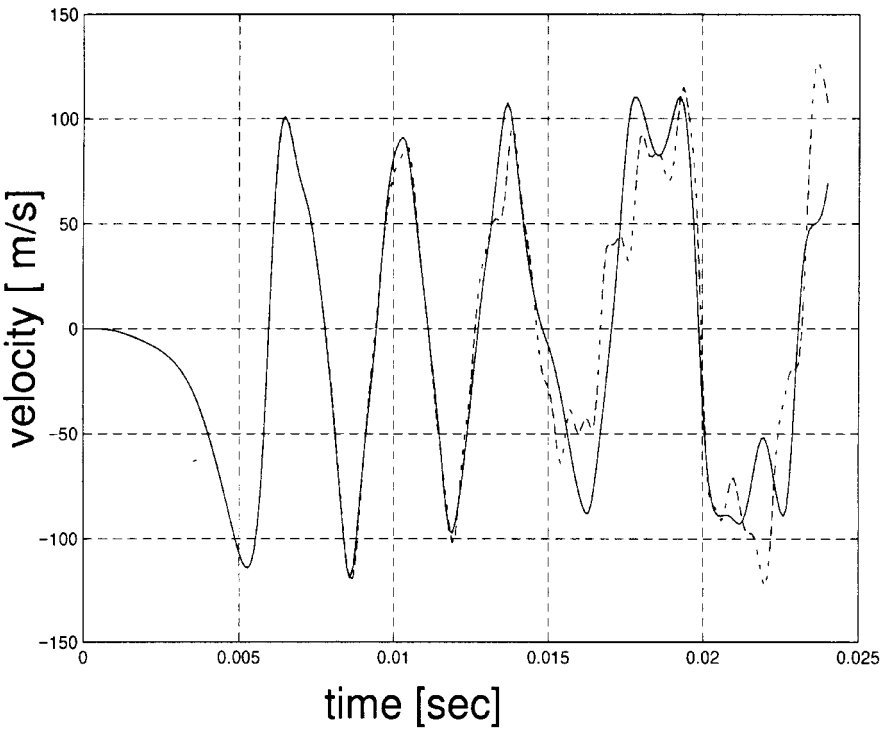

Figure 19. Time history of the mid-span vertical velocity of the arch for the energy–preserving (dashed line) and decaying (solid line) schemes

ratio $\nu = 0{\cdot}0$, material density $\rho = 1{\cdot}0\,\mathrm{kg/m^3}$, and a thickness $t = 1{\cdot}0\,\mathrm{m}$. At infinitesimal impact speed the problem is linear, and the exact solution consists of a compressive wave travelling at a constant speed $a = \sqrt{E/\rho} = 1{\cdot}0\,\mathrm{m/s}$. Due to symmetry, only the upper-half of the bar was modelled. At time $t = 0\,\mathrm{s}$, all points of the bar were given an initial velocity v_0, and all nodes on the left edge of the bar were constrained to a zero displacement. Symmetry conditions were applied along the centre line of the bar.

At first, the energy–preserving scheme will be used to model this problem, with a constant time step size $\Delta t = 0{\cdot}01\,\mathrm{s}$. Three meshes of 200, 400, and 800 9-noded elements of equal length will be used in this study. Figure 14 shows the axial stress distribution in the bar at time $t = 2{\cdot}56\,\mathrm{s}$, at which time the compressive wave is located at a distance $x = 2{\cdot}56\,\mathrm{m}$ from the left end of the bar. For clarity, the figure focuses on the mid-section of the bar, from $x = 2$ to 3 m. Note the presence of increasingly large amplitude oscillations as the mesh is refined.

Next, the energy–decaying scheme was used with identical time step and meshes. Figure 15 shows the corresponding results. Although oscillations are still present, the results markedly improve with mesh refinement: the amplitude of the oscillations is reduced, and the wave's front location is captured with increasing accuracy. With the finest mesh, highly damped, small amplitude oscillation are present on both sides of the front.

In an attempt to characterize the quality of the solutions presented above, the total area defined by the difference between the various solutions and the exact solution was computed (all areas were

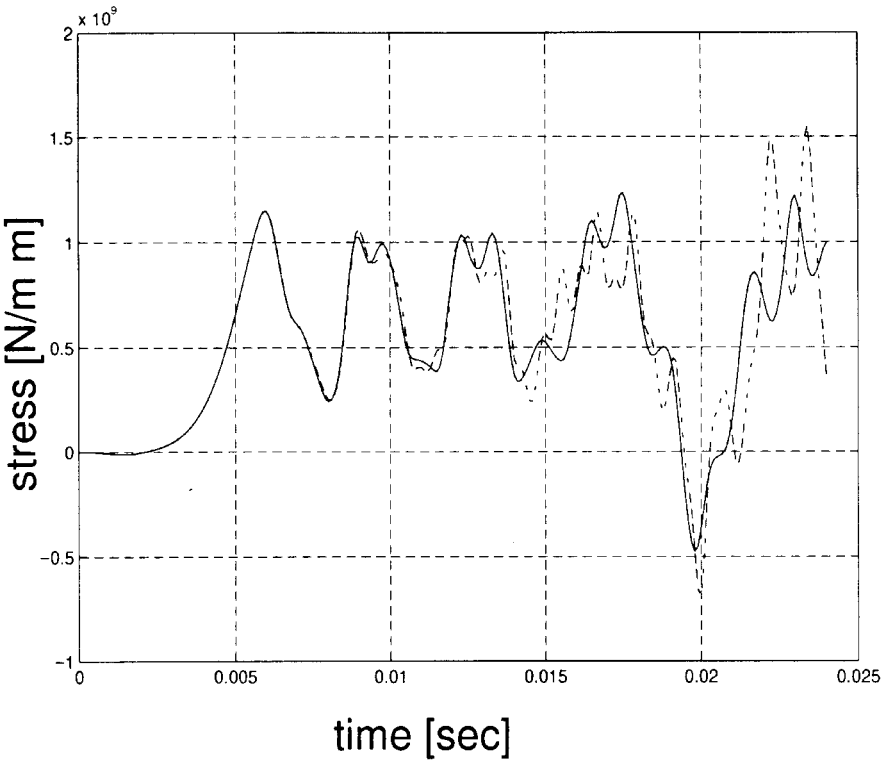

Figure 20. Time history of the mid-span vertical stress of the arch for the energy-preserving (dashed line) and decaying (solid line) schemes

added in absolute value). Figure 16 shows this error index plotted as a function of the number of degrees of freedom in the model. The convergence of the results for the energy–decaying scheme is clearly seen in this figure, as opposed to the predictions of the energy–preserving schemes for which oscillations increase with mesh refinements. This clearly indicates the critical need for the high–frequency numerical dissipation provided by the energy–decaying scheme.

5.3. The arch problem

The last numerical example deals with the dynamic response of a simply supported arch subjected to time-varying loads. Figure 17 shows the geometry of the problem: the arch radius of curvature is $R = 2{\cdot}54\,\mathrm{m}$, its depth $h = 5{\cdot}08\ 10^{-2}\,\mathrm{m}$, thickness $t = 1\,\mathrm{m}$, and $\Theta = 0{\cdot}245\,\mathrm{rad}$. The span of the arch is then $L = 1{\cdot}2446\,\mathrm{m}$, and a vertical concentrated load is applied at quarter span. Material properties are: Young's modulus $E = 69\,\mathrm{GPa}$, Poisson's ratio $\nu = 0{\cdot}3$, and material density $\rho = 2607\,\mathrm{kg/m^3}$. The mesh consists of 56 9-noded elements, with two elements through the depth of the arch.

The time history of the applied loading is selected as $P(t) = 10\ [1 - \cos\ (2\pi t/0{\cdot}02)]\,\mathrm{MN}$. The dynamic response was simulated for $0{\cdot}025\,\mathrm{s}$ with a constant time step size $\Delta t = 10^{-4}\,\mathrm{s}$. Figures 18, 19, and 20 show the time history of the arch mid-span vertical displacement, vertical velocity,

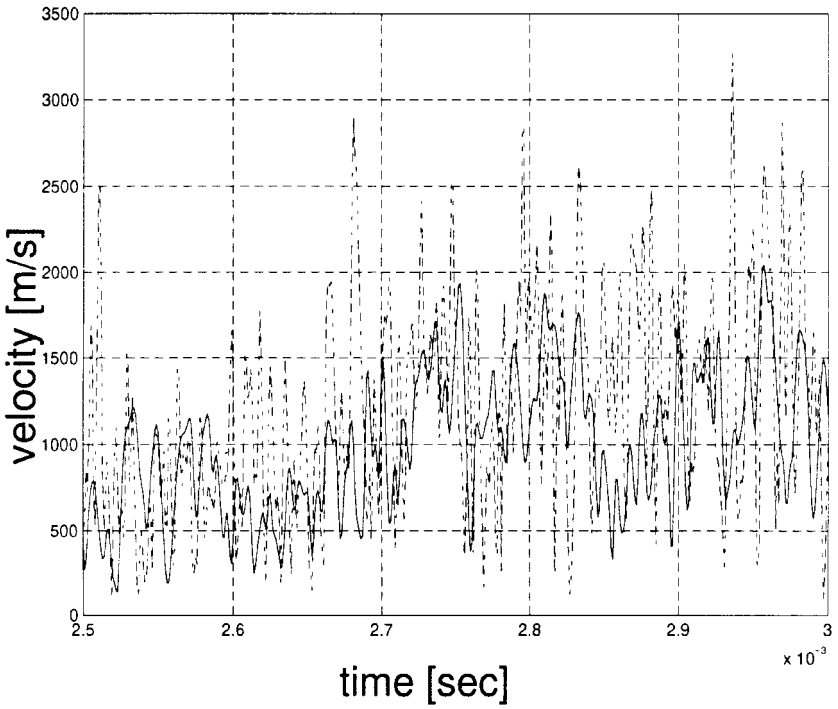

Figure 21. Time history of the norm of the velocity vector at three-quarter span using the energy–preserving (dashed line) and decaying (solid line) schemes

and horizontal stress, respectively, for both energy–preserving and decaying schemes. After about 5×10^{-3} s the arch snaps through and after several oscillations about that configuration snaps back at a time of about 20×10^{-3} s. Initially, the predictions of energy–preserving and decaying schemes are in excellent agreement. However, due to the different accuracy of the schemes (Δt^2 vs. Δt^3) discrepancies are observed as the simulation proceeds.

Finally, the high-frequency numerical dissipation characteristics of the energy–decaying scheme will be demonstrated. The above arch problem is slightly modified: a lumped mass is added at the arch mid-span by increasing 20 times the material density of the four elements at mid-span. The quater span loading is now of a more impulsive nature: the load linearly increases from zero to 10^9 N in 10^{-04} s, is then held constant for 5×10^{-04} s, and finally ramps down to zero in 6×10^{-04} s. For times greater than 12×10^{-04} s, no loading is applied. A constant time step size $\Delta t = 10^{-6}$ s is used for the simulation. The inertial forces associated with the mid-span lumped mass considerably increase the maximum displacements both during the snap through, and when the arch snaps back. Figure 21 shows the norm of the three-quarter point velocity vector for both energy–preserving and decaying schemes, from time $t = 2{\cdot}5$ to $t = 3{\cdot}0 \times 10^{-03}$ s. The predictions of the energy–preserving scheme clearly exhibit very high-frequency oscillations that have been damped out by the energy–decaying scheme. This fact is confirmed by Figure 22 which show the fast Fourier transform of the time history in Figure 21.

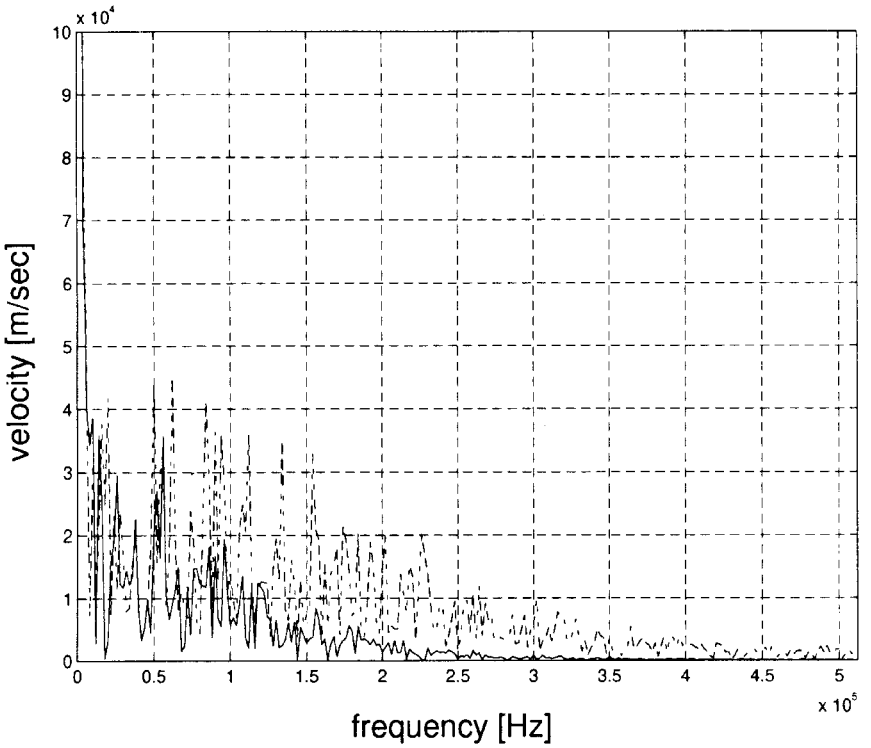

Figure 22. Fast Fourier transform of the norm of the velocity vector at three-quarter span using the energy-preserving (dashed line) and decaying (solid line) schemes

6. CONCLUSIONS

In this paper, two time-integration schemes were presented for non-linear elastodynamics. First, an energy–preserving scheme was presented for which a discreted energy conservation statement was proved, resulting in unconditional stability for the non-linear problem. The scheme presents no numerical dissipation and is second-order accurate. Next, a novel energy–decaying scheme was developed which implies a discrete energy decay inequality, resulting again in unconditional stability for the non-linear problem. The scheme presents high-frequency numerical dissipation and is third-order accurate.

Numerical examples have been presented to validate the proposed integration schemes and demonstrated their accuracy and efficiency. The energy–decaying scheme clearly provides the unconditional stability and high-frequency numerical dissipation characteristics required for the analysis of non-linear elasto-dynamic problems.

REFERENCES

1. Hughes TJR. Analysis of transient algorithms with particular reference to stability behavior. *Computational Methods for Transient Analysis*; North-Holland: Amsterdam, 1983;67–155.

2. Newmark NM. A method of computation for structural dynamics. *Journal of the Engineering Mechanics Division* 1959;**85**:67–94.
3. Hughes TJR. *The Finite Element Method*; Prentice-Hall: Englewood Cliffs, NJ, 1992.
4. Hilber HM, Hughes TJR, Taylor RL. Improved numerical dissipation for time integration algorithms in structural dynamics. *Earthquake Engineering and Structural Dynamics* 1977;**5**:282–292.
5. Chung J, Hulbert GM. A time integration algorithm for structural dynamics with improved numerical dissipation: the generalized-α method. *Journal of Applied Mechanics* 1995;**122**:254–266.
6. Simo JC. Tarnow N. The discrete energy-momentum method. Conserving algorithms for nonlinear dynamics. *Zeitschift für Angewandte Mathematik und Physik* 1992;**43**:757–792.
7. Bauchau OA, Damilano G, Theron NJ. Numerical integration of nonlinear elastic multi-body systems. *International Journal for Numerical Methods in Engineering* 1995;**38**:2727–2751.
8. Johnson C. *Numerical Solutions of Partial Differential Equations by the Finite Element Method*; Cambridge University Press: Cambridge, 1987.
9. Johnson C, Nävert U, Pitkäranta V. Finite element methods for linear hyperbolic problems. *Computer Methods in Applied Mechanics and Engineering* 1984;**45**:285–312.
10. Johnson C, Szepessy V. Convergence of a finite element method for a nonlinear hyperbolic conservation law. *Technical Report 1985-25*, Mathematics Department, Chalmers University of Technology, Göteborg, Sweden, 1985.
11. Hughes TRJ, Hulbert M. Space-time finite element formulations for elastodynamics: Formulation and error estimates. *Computer Methods in Applied Mechanics and Engineeering* 1988;**66**:339–363.
12. Hulbert M. Space-time finite element methods for second-order hyperbolic equations. *Ph.D. Thesis*. Stanford University, 1989.
13. Lanczos C. *The Variational Principles of Mechanics*; Dover Publications: New York, 1970.
14. Malvern LE. *Introduction to the Mechanics of a Continuous Medium*; Prentice-Hall: Englewood Cliffs, NJ, 1969.

